IEEE Access
Multidisciplinary | Rapid Review | Open Access Journal

Received 1 March 2024, accepted 21 March 2024, date of publication 1 April 2024, date of current version 5 April 2024.

Digital Object Identifier 10.1109/ACCESS.2024.3383774

RESEARCH ARTICLE

A Suspended Aerial Manipulation Avatar for Physical Interaction in Unstructured Environments

FANYI KONG[1], (Graduate Student Member, IEEE), GRAZIA ZAMBELLA[1], (Member, IEEE), SIMONE MONTELEONE[1], GIORGIO GRIOLI[1,2], (Member, IEEE), MANUEL G. CATALANO[2], (Member, IEEE), AND ANTONIO BICCHI[1,2], (Fellow, IEEE)

[1]Centro di Ricerca E. Piaggio e Dipartimento di Ingegneria dell'Informazione, Università di Pisa, 56126 Pisa, Italy

[2]Fondazione Istituto Italiano di Tecnologia, 16163 Genoa, Italy

Corresponding author: Fanyi Kong (kong.fanyi95@gmail.com)

This work was supported in part by European Commission Horizon 2020 Research and Innovation Program as part of the Projects Socio-physical Interaction Skills for Cooperative Human-Robot Systems in Agile Production (SOPHIA) Self-Reconfiguration of a Robotic workcell for the Recycling of Electronic Waste (ReconCycle) under Grant 871237 and Grant 871352, and in part by Chinese Scholarship Council under Grant 202006120005.

ABSTRACT This paper presents an aerial platform capable of performing physically interactive tasks in unstructured environments with human-like dexterity under human supervision. This aerial platform consists of a humanoid torso attached to a hexacopter. A two-degree-of-freedom head and two five-degree-of-freedom arms equipped with SoftHands provide the requisite dexterity to allow human operators to carry out various tasks. A robust tendon-driven structure is purposefully designed for the arms, considerably reducing the impact of arm inertia on the aerial base in motion. In addition, tendons provide flexibility to the joints, which enhances the robustness of the arm preventing damage in interaction with the environment. To increase the payload of the aerial system and the battery life, we use the concept of Suspended Aerial Manipulation, i.e., the flying humanoid can be connected with a tether to a structure, e.g., a building, a fixed bracket, a supporting crane, or a larger airborne carrier. Importantly, to maximize portability and applicability, we adopt a modular approach exploiting commercial components for the aerial base hardware and autopilot. We develop an outer stabilizing control loop to maintain the attitude, compensating for the tether force and for the humanoid head and arm motions. The humanoid can be controlled by a remote operator, thus effectively realizing a Suspended Aerial Manipulation Avatar. The proposed system is validated through experiments in indoor scenarios reproducing post-disaster tasks.

INDEX TERMS Aerial manipulation, dual-arm robot, teleoperated avatar, cable-suspended robot.

I. INTRODUCTION

The increasing prominence of aerial robots in the realm of mobile robotics is propelled by recent advancements in unmanned aerial vehicle (UAV) technology. The inherent capability of flight provides advantages not present in conventional ground-based robotic platforms, facilitating rapid deployment in elevated terrains, post-catastrophe environments, and other distant and hazardous locations. Beyond passive sensing, researchers actively explore the potential of UAVs for environmental interaction. The amalgamation of end-effectors with robotic arms, or collectively manipulators, coupled with the inherent aerial maneuverability of UAV platforms, leads to the conceptualization and realization of Unmanned Aerial Manipulators (UAMs).

UAMs have undergone scrutiny for various applications, including industrial pipeline inspection [1], wind turbine blade cleaning [2], and tasks involving torsion, such as screwing bolts, replacing light bulbs, and crop harvesting [3]. The versatility of UAMs extends to potential applications in post-disaster response scenarios. A comprehensive assessment of the evolution and prevailing trends in UAMs is

The associate editor coordinating the review of this manuscript and approving it for publication was Turgay Celik.

available in [4]. Furthermore, [5] proposes a review of design techniques, while the authors of [6] present a survey covering mechanics, modeling, and control architectures pertinent to UAMs.

Within the realm of UAMs, dual-arm aerial platforms constitute a substantial branch. Key advantages of these platforms include heightened dexterity and enhanced manipulation capabilities resulting from an expanded workspace. Furthermore, the dual-arm structure offers the potential to partially eliminate reaction wrenches on the platform through compensatory movements, as illustrated in [7]. Table 1 compiles recent dual-arm aerial platforms, presenting a comparative analysis of their primary technical specifications. This analysis encompasses parameters such as arm weight, payload capacity, Degrees of Freedom (DoFs) of the arms, and the incorporation of compliance features. In [7] (row 1 of Table 1), the authors present a hexacopter-based aerial manipulator with a lightweight arm design implemented with an aluminum frame. In [8] (row 2), compliance is introduced into the lightweight dual-arm design by incorporating a compact spring-lever transmission mechanism. The authors in [9] (row 3) investigate bimanual aerial manipulation tasks with one arm grabbing to a fixed point on a lightweight and compliant dual-arm aerial manipulation robot. An open-source, low-cost dual-arm system for aerial manipulation is presented in [10] (row 4). The authors of [11] (row 5) present a dual-arm UAM with an anthropomorphic design and successfully assemble two workpieces in an outdoor experiment. The authors of [12] (row 6) and [13] propose an aerial platform with two 4-DoF arms and apply it to valve turning. In [14] (row 7), the readers can find a commercial version of a dual-arm aerial manipulator.

To avoid collisions between UAVs and obstacles in complex environments and dynamic turbulence caused by ground effects, the long-reach configuration has been introduced in aerial manipulator design. The long-reach configuration involves suspending the robotic manipulator from the UAV using a long rigid or flexible link (e.g., long wires) rather than fixing it directly to the UAV. References [15], [16], and [17] present several aerial manipulator prototypes that attach lightweight dual arms to the aerial platform in long-reach configuration via a passive link and their industrial applications in the pipeline inspection and sensor device installation. Reference [18] presents a long-reach manipulator suspended by two strings applied to installing helical bird diverters on power lines. In these prototypes, the manipulators are passively suspended from the UAVs like pendulums. The swinging motion naturally introduced is seen as a disturbance compensated for by the UAV control. In [19], the authors install non-vertical ducted fans on the suspended gripper module to suppress the string swing effect, In addition, they used a winch to control the distance between the gripper and the multi-rotor platform. The authors of [20] present a similar cable-Suspended Aerial Manipulator (SAM) actuated by winches and non-vertical propulsion units, and propose an oscillation damping control in [21]. When analyzing the system model, the authors of these two prototypes considered the aerial manipulator independently of the vehicle, assuming it is suspended from a fixed point and suppressed its swing by controlling the propulsion device.

Teleoperation is a prevalent method of robot control that enables human supervision and intervention in task execution through a primary-secondary mode. Researchers have also explored its application in aerial manipulation. The authors of [22] introduce a passivity-based control framework for the teleoperation of a kinematically redundant aerial platform. The aerial base is equipped with a monocular camera, and its perspective is adjusted using the platform redundancy. Task execution involves switching among control options facilitated by a 2-DoF joystick. In [23], the authors introduce a telepresence system employing visual-inertial feedback to construct a real-time virtual representation of the workspace for the operator within virtual reality (VR). Similarly, the authors of [24] and [25] present comparable teleoperation system designs, featuring the presentation of a digital twin of the aerial robot and the remote environment in virtual reality to the user through a head-mounted display. Notably, in [24], manipulator movement is controlled by trackers worn by the operator, while in [25], a set of joysticks serves as the input device.

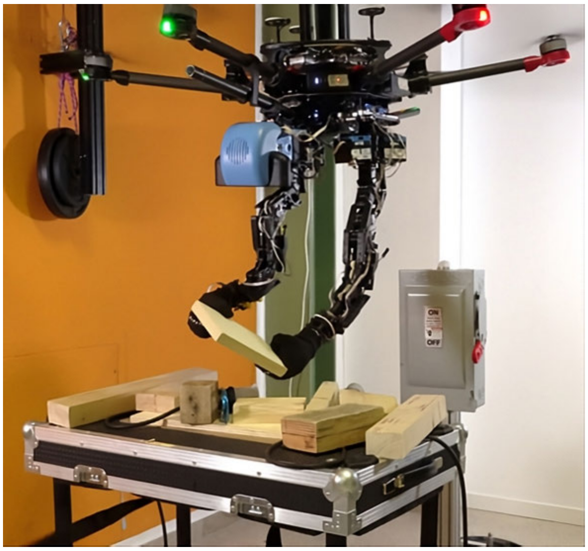

FIGURE 1. Prototype of the aerial platform used for aerial teleoperation. It is composed of a DJI hexacopter base, two 5-DoF arms based on novel soft articulated joints, two SoftHands (derivation of the PISA/IIT SoftHand [26]), and a 2-DoF head.

In our previous work [27], on which this manuscript is partially based, we have introduced a novel design of a hexacopter equipped with an anthropomorphic torso comprising two soft-articulated 5-DoF arms, two SoftHands, and a 2-DoF head. A notable innovation in the arm design has been introduced, involving the integration of tendons and elastic bands. This permits the positioning of the actuation unit away from the rotation shafts and increases the robustness of the system against accidental shocks.

TABLE 1. Examples and primary characteristics of dual-arm aerial platforms in the literature.

Reference	Aerial Base	Arm Weight	Arm Payload (each)	Arm DoF (each)	Compliant	End Effector	Head	Open-Source	Simulator	Teleoperation
[7]	Hexacopter	1.8 kg total	0.75 kg	5	No	Gripper	Fixed Camera	No	MATLAB	6-DoF mouse
[8]	Hexacopter	1.3 kg total	0.2 kg	4	Yes	Gripper	Fixed Camera	No	No	6-DoF Mouse
[9]	Hexacopter	1.0 kg total	0.3 kg	3	Yes	Gripper	No	No	No	No
[10]	Hexacopter	0.5 kg each	NA	4	No	Multiple Gripper	Fixed Camera	Yes	OpenRave	Gamepad, Joystick, GUI
[11]	Hexacopter	1.9 kg total	NA	4	No	Gripper	Fixed Camera	No	MATLAB	No
[12]	Quadrotor	NA	NA	4/2	No	Gripper	No	No	No	No
[14]	Hexacopter	NA	NA	NA	No	Gripper	NA	Commercial	No	NA
proposed	Hexacopter	2.85 kg each	2 kg	5	Yes	SoftHand [26]	Movable	Yes	Gazebo	VR

The SoftHands [26] have been adapted to match the aerial platform design to enhance the grasping and manipulation performance, owing to their capacity to conform the grasp to the shape of objects. In contrast to the approaches outlined in [23], [24], and [25], which replicate the work scene with the digital twin of the robot in a third-person perspective, our design employs a binocular camera in conjunction with a VR headset. This setup enables the human operator to gain an intuitive first-person view of the workspace, complete with depth information. Moreover, the 2-DoF head design allows the synchronization of the movements of the robot head with those of the operator, circumventing the need for intricate perspective switching and enhancing the operator's understanding of the workspace. Drawing inspiration from [28] and [29], we employ two handheld joysticks to track the movement of the operator's hands, controlling the robotic arms to follow and replicate human movements.

Here, we extend [27] by integrating the aerial platform design with a variable-length suspension mechanism for weight compensation (see Fig. 1), effectively making it a Suspended Aerial Manipulation Avatar (SAM-A). This design, inspired by [20], considerably extends the system flight duration and endows it with the versatility to attach to various carriers such as buildings, fixed brackets, cranes, or manned aerial vehicles, facilitating access to areas where UAV operations may be restricted. However, our approach overcomes some of the limitations of [20] by introducing non-fixed compensation to preserve freedom of motion for the aerial platform. Additionally, we present an aerial base stabilizing controller that takes into account the motion of the humanoid torso and the influence of the tethering system. This controller is integrated within a teleoperation framework, enabling human operators to control the platform in an immersive and intuitive manner. Moreover, our system adopts a modular approach, utilizing a commercial UAV as the aerial base and offering open-source design, providing an easily replicable solution and contributing to the portability and applicability of our aerial platform modeling and control design to similar configurations. The efficacy of the proposed controller is validated through experiments conducted within an indoor test rig. A series of representative experiments simulating scenarios relevant to post-disaster reconstruction efforts are conducted to demonstrate the functionality and effectiveness of our design.

We organized the paper as follows. Section II explains the motivation and provides an overview of our design. Section III covers the mechatronic design of the system. Section IV describes the system model. Section V presents the control architecture. Finally, Section VI displays the experimental setup and results, and Section VII concludes the paper.

II. CONCEPT

After a disaster such as an earthquake, a flood, a fire, or a landslide, robots often need to access high-risk environments as observers and operators. Ground robots can be hampered by debris and objects on the ground, and safely surpassing them is not always trivial. On the contrary, a robot capable of approaching mission areas from the air is intrinsically immune to such obstacles and, therefore, greatly enhances the possibility of inspecting and intervening in adverse surroundings for humans. However, limited flight time and payload, as well as unknown challenges and potential threats in the unstructured working space, are some of the notable constraints limiting the application of aerial robots in practical scenarios.

In addition to relying on advancements in battery technology for extended flight time, a common strategy involves reducing the weight of the aerial manipulator during the mechanical design phase. Researchers often achieve this by selecting low-density, high-strength materials and navigating a compromise between degrees of freedom, functionality, and overall mass. However, a notable departure from conventional non-grounded robots is the concept of a cable-suspended aerial manipulator, introduced in [20]. In this paradigm, an aerial manipulator is designed to be suspended from an aerial carrier, such as a manned aerial vehicle or a crane.

The carrier bears a significant portion of the manipulator weight, leading to a substantial increase in payload capacity and aligning with the overarching objective of prolonging flight time.

UAVs are inherently unstable systems, relying on continuous and substantial rotor efforts to maintain stability. Compared with ground robots, the disturbances to aerial manipulators brought by operations may have a more devastating impact, making it particularly challenging to conduct interactive tasks in unknown environments where there are more potential disturbances. Therefore, when designing aerial manipulators, particular attention must be dedicated to minimizing those disturbances caused by arm movement and interaction. One of the lessons in the arm design with application to aerial manipulation is to constantly maintain their Center of Mass (CoM) close to the CoM of the UAV. Consequently, it is imperative that the base of the arm carries the majority of its weight. Additionally, compliance can be integrated into the design, which can prevent the arm from breaking during accidental collisions between the robot and the environment and mitigate the impact on the stability of the UAV caused by sudden and impulsive loads encountered during manipulation. Furthermore, in order to tactfully respond to various situations that may arise in unknown environments, a practical strategy is to maintain human supervision of the aerial manipulator rather than relying entirely on its autonomy.

A. PROPOSED APPROACH

Taking inspiration from SAM [20] and the aerial manipulators described in Table 1, we aim to design a Suspended Aerial Manipulation Avatar for inspection and intervention in unstructured environments in which human intelligence is relocated directly in the aerial platform working space. It is designed for deployment across diverse scenarios, including cities after earthquakes, floods and fires, canyons, vertical mines, sinkholes, and mountainous areas after landslides, utilizing various carriers such as cranes, fixed structures, and airborne carriers like helicopters (see Fig. 2).

In contrast to the approach proposed in [20], which relies entirely on the tether for lifting the entire weight of the robot but confines its motion to a spherical surface, we address the challenges of flight duration and load capacity through the implementation of a variable-length suspension system for gravity compensation. This system partially offsets the overall weight, enabling the aerial base to utilize its thrusters for various maneuvering operations, including ascending, descending, and translating. This design preserves the inherent characteristics of the aircraft and significantly upholds the independence of the aerial base from the cable suspension system. Consequently, it allows for movement within a larger workspace and facilitates more agile operations by coordinating the aerial base motion with the arm motion, rather than relying solely on the degrees of freedom of the arms.

The arms and head are affixed to the underside of the UAV, configured to mimic the upper body of a human but with a downward orientation. The dual arms are symmetrical to reduce the burden on the rotors. A tendon-elastic-band-pulley structure is applied to the arm design to meet the requirements given by stability and robustness. This design choice allows the actuation units, which contribute significantly to the overall weight, to be situated in close proximity to the body on the aerial platform. Moreover, the joints comprised of disarticulated components are intentionally designed to be less rigid owing to the incorporation of tendons and elastic bands. A similar approach to compliance is adopted in the head joints to mitigate the potential accidental impacts. This design strategy enhances the overall adaptability and safety of the aerial manipulator system. Finally, two SoftHands are employed as end-effectors. The SoftHands have a unique design that consents to many dexterous grasps with a sole actuation unit. When grabbing objects with conventional shapes, standard grippers would be more reliable. The SoftHands, on the other hand, proved to be more adaptable to performing the various grasps [26] resulting from employing the aerial manipulator in unstructured environments in which the shape of objects is not known in prior. Moreover, the mechanics of the hands are intrinsically robust against accidental collisions, making the use in teleoperation safe and effective.

In addition to the humanoid design of the platform, we integrate a suite of VR user interfaces for first-person visual perception and control. With the synchronization of the first-person perspectives and movements between the operator and the robot, the teleoperation is intuitive and straightforward. Human operators can engage in immersive work experiences akin to being physically present in the robot operating environment, allowing them to efficiently manage diverse tasks and respond promptly to emergent situations. The combination of this teleoperation experience, along with the humanoid robotic torso equipped with dexterous hands, effectively positions this aerial robotic platform as an "Avatar."

The aerial base employed is a conventional commercial hexacopter equipped with parallel thrusters, with the proposed control system designed to run on top of it. While its under-actuated nature may introduce complexity in decoupling and stabilization compared to fully-actuated drones, it offers the distinct advantages of simplicity and reliability. Moreover, the technology associated with such hexacopters is thoroughly researched and extensively commercialized, enhancing the feasibility of our proposed solution for widespread application across various scenarios.

III. PLATFORM DESIGN

A. MECHANICAL DESIGN

As discussed above, the aerial avatar is designed to access unstructured environments and manipulate objects. The main

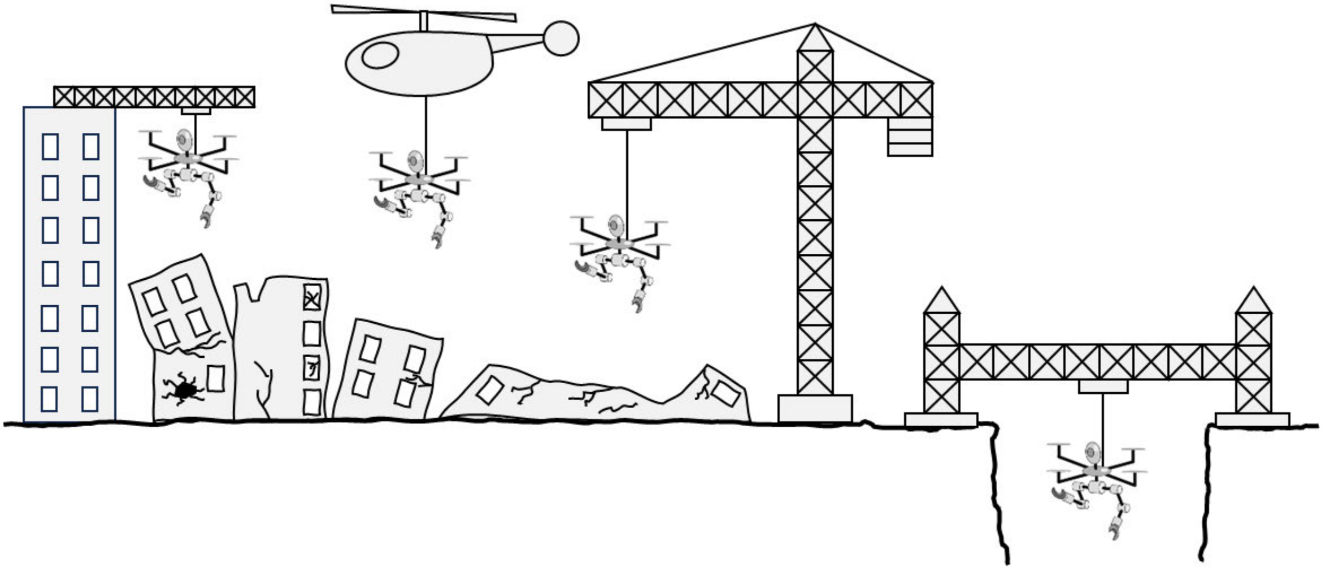

FIGURE 2. **Concept of SAM-A. The suspended aerial manipulation avatar is designed for operation in highly unstructured environments, such as a city after a disaster (left) or a sinkhole (right). An external support structure such as a building, a helicopter, or a crane improves payload bearing and autonomy, while an independent propulsion system stabilizes the bi-manual manipulating platform.**

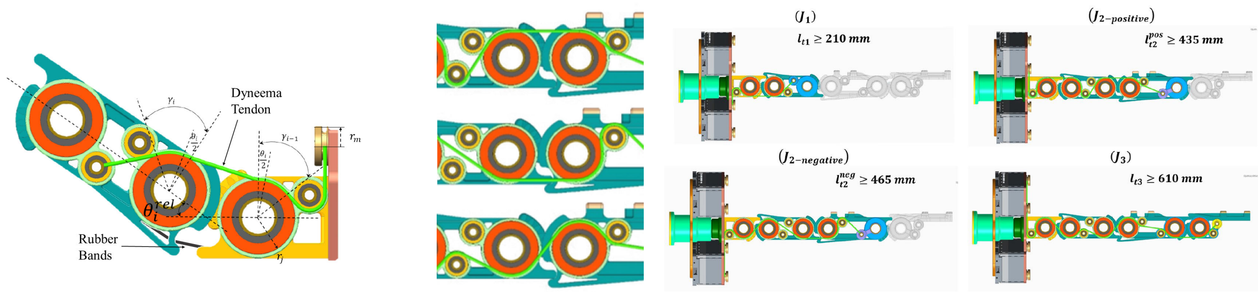

(a) (b) (c)

FIGURE 3. **a) Configuration of the joints. The figure shows the kinematic relations between the motor and joint rotation and presents the two axes around which the joint rotates. The elastic bands keep the joint in position while the tendon drives it. b) Routing of the tendons inside a joint. From top to bottom, the positive configuration closes the joint, the negative configuration opens it, and the neutral configuration exerts no action. c) Routing of the four tendons to achieve the differential actuation of the joints.**

mechanical components of the systems are the hexacopter aerial base, which constitutes the body of the platform, the arms, the hands, the head, and the compensation system. The open-source materials are available online.[1]

1) AERIAL BASE

While the tether can compensate for a significant portion of the weight of the aerial manipulator, enhanced drive capabilities are still necessary for the aerial base. This requirement translates to faster response times and improved dynamic performance. To enhance portability and broaden the applicability of the system, the aerial base is constituted by a DJI Matrice 600 Pro.[2] The hexacopter weighs 9.5 kg and lifts a maximum recommended takeoff load of 15.5 kg. Therefore, the net recommended payload is 6 kg. Temporarily overboosting the propellers can increase the maximum load to 10 kg. The dimensional encumbrance in operative working conditions is 1668 mm × 1518 mm × 727 mm with propellers, frame arms, and GPS antennas unfolded.

2) DUAL ARMS

The arm design principle is governed by three primary considerations: dexterity, total weight, and weight distribution. While increased degrees of freedom contribute to greater dexterity, they concurrently add weight to the arms, introducing disadvantages for aerial base control. Thus, striking a balance between dexterity and total weight is generally necessary. Furthermore, the distribution of weight must be taken into account to prevent substantial changes in the CoM and minimize interference moments on the aerial base resulting from arm movements.

To achieve these goals, the arm design is inspired by the tendon-driven manipulators that exist in the literature [30],

[1]https://www.naturalmachinemotioninitiative.com/aerial-alter-ego
[2]https://www.dji.com/it/matrice600-pro

particularly the phalanges of the IIT/Pisa SoftHand [26]. It introduces tendon-driven actuation with a tensegrity structure implemented with elastic cables into the elbow design, and presents two main advantages. First, unlike conventional robotic arms with direct transmission such as the ones in [7] that place the motors at the joints, the tendon design allows most motors, which account for considerable weight, to be placed at the base of the arm. This design optimizes weight distribution for aerial manipulator applications, bringing the CoM of the arm closer to the aerial base and reducing the weight of the arm links, thereby minimizing its backlash on the body. The latter is that the elastic bands present soft ligaments to the joints, which improves the robustness of the arm and protects it in the case of accidental collisions [31]. Based on this design, the elbow is actuated by tendons and has three rotational DoFs to reduce CoM shifting during arm grabbing and lifting, thereby further improving stability. Two motors located at the base of the arm and at the wrist drive the shoulder and wrist joints independently. In total, the arm has five DoFs, including one for the shoulder, three for the elbow, and one for the wrist. The kinematic definition of the arm is reported in Table 2.

TABLE 2. Denavit-Hartenberg chain of each arm.

Link	a	α	d	θ
1	0	$-\pi/2$	0	$-\pi/2+\theta_1$
2	0.110	0	0	$-\pi/2+\theta_2$
3	0.140	0	0	θ_3
4	0	$\pi/2$	0	$\pi/2+\theta_4$
5	0	0	0.220	θ_5

As shown in Fig. 3a, the joint is created with two pulleys and toothed profiles. A tendon made of Dyneema fiber is wrapped around these two pulleys and connected to a motor at the bottom of the arm. It deforms less than one percent at nominal load and is strong enough to drive the arm linkage to follow the toothed profile of the pulleys as the motor rotates, resulting in a moving center of rotation. A set of rubber elastic bands contributes to the structural integrity, ensuring that the toothed profiles stay in position during normal rotation and under accidental impacts. The transmission ratio from the motor to the shaft joint is

$$r = \tfrac{r_m}{r_j}, \tag{1}$$

where r_j is the radius of the joint pulley, and r_m is the radius of the pulley connected to the motor. It is worth noticing that the motion of the elbow joint is achieved by two separate rotations. An elbow joint movement of θ_i is generated by rotations of $\theta_i/2$ along two different axes of the pulleys constituting the joint.

The design incorporates a system where a single tendon can only exert pull force, necessitating at least two tendons to enable movement in two directions for one joint. Three configurations of tendon application are employed when wrapping around a joint, as illustrated in Figure 3b. In the positive configuration, the tendon closes the joint; in the negative configuration, it opens it, while in the neutral configuration, it merely passes through the joint without generating any torque.

Utilizing these configurations, four tendons drive three elbow joints through a differential arrangement, as depicted in Figure 3c. The first tendon is positively wrapped around the first elbow joint J_1. Conversely, the second tendon passes around J_1 in a negative arrangement and, simultaneously, positively around J_2. The third cable is neutral on J_1 and negative on J_2. Finally, the fourth tendon is neutral around J_1 and J_2 and positive around J_3. The closing action on J_3 is facilitated by elastic rubber cables and is thus passive. The elastic behavior on the joint is experimentally evaluated through traction tests, approximating a linear dependence between force and elongation within the working range. When appropriately controlled, this tendon displacement configuration enables independent movement of all the joints.

The kinematic projection between the arm joints q_a (q_{ra} for the right arm and q_{la} for the left) and the drive motors $q_m \in \mathbb{R}^6$ is

$$q_a = F \cdot q_m\,, \tag{2}$$

where

$$F = \begin{bmatrix} 1 & 0 & 0 & 0 & 0 & 0 \\ 0 & r & -r & 0 & 0 & 0 \\ 0 & 0 & r & -r & 0 & 0 \\ 0 & 0 & 0 & 0 & r & 0 \\ 0 & 0 & 0 & 0 & 0 & 1 \end{bmatrix}. \tag{3}$$

The arm links are made by 3D printing with a lightweight hollow frame design. Fig. 4 shows the dual arms assembly. The whole arm weighs approximately 2.85 kg, divided by around 2.0 kg on the shoulder and 0.85 kg on the rest of the arm (including a 0.35 kg hand). Ideally, without considering the aerial base, the end of the arm can output 6 Nm of maximum torque and 30 N of maximum force.

3) HANDS

For each arm, a lightweight version of PISA/IIT Softhand [26] is equipped for manipulation. It is an optimal solution that compromises weight, dexterity, and compliance for aerial manipulation applications. The SoftHand is a 19 DoF system weighing around 0.35 kg, which is actuated by a single motor and a tendon that wraps around all the fingers, allowing maximum holding torque of 2 Nm and maximum holding force of about 20 N. Their employment enhances the capabilities of the aerial avatar to handle objects of different shapes and dimensions, thanks to their intrinsic adaptability and softness. For more information, the authors suggest referring to [26].

4) HEAD DESIGN

The head is located at the bottom of the aerial base and in the middle of the two arms, installed on the landing gear of the UAV through a four-bar linkage. The head design

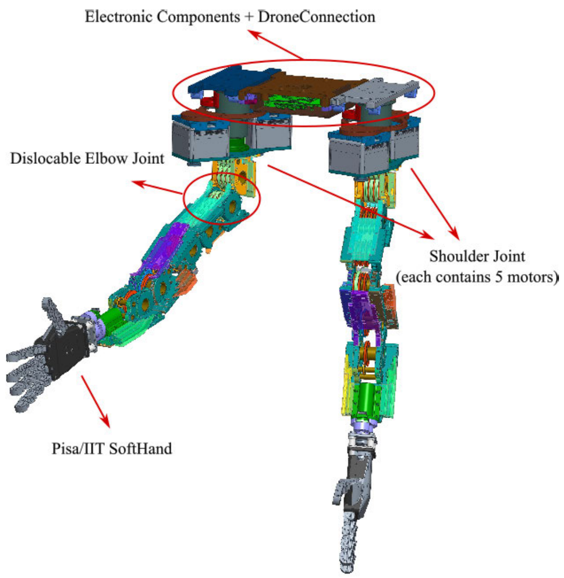

FIGURE 4. Description of the dual arms of the platform. The picture points out the position of the electronics, the localization of the actuation units of both arms, the articulated joints, and the SohtHands employed as end-effectors.

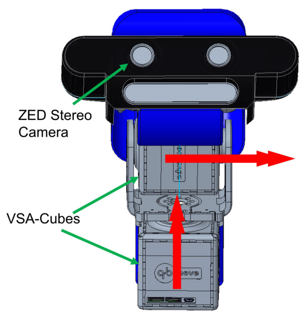

FIGURE 5. 2-Dofs head, showing the direction of rotation and the position of the binocular camera.

is similar to the one already employed for Alter-Ego [28]. It consists of a 2 DoFs neck and a Zed Mini Stereo Camera to "see" the workspace while teleoperating (see Fig. 5). The neck joints employ two VSA-Cubes [32] as actuation units, which introduce compliance to cope with possible impacts. The neck allows rotating the head around the direction of pitch and yaw, as its kinematics model defined in Table 3. The choice is related to the sensations that an operator experiences while commanding such robotic platforms. Experimentally, we found that yaw and pitch were fundamental to avoiding nausea and disorientation during teleoperation. Conversely, the absence of a rolling movement is not experienced as stressed by operators; therefore, we eliminated it to reduce the head weight to approximately 1.5 kg.

TABLE 3. Denavit-Hartenberg chain of the head.

Link	a	α	d	θ
1	0	$\pi/2$	0.056	$\pi/2+\theta_1$
2	0.094	0	0	$0.52+\theta_2$

5) COMPENSATION SYSTEM

The compensation system adopts a variable-length design, allowing the cable length to change while exerting tension on the aerial platform. It consists of a force generator and a force adjuster. The compensation force is generated by the force generator and then adjusted by the force adjuster before being applied.

Considering the impact on system dynamics, two alternative configurations are designed as force generators: counterweight or constant force springs, as demonstrated in Fig. 6a and Fig. 6b. The counterweight design involves a counterweight and a pulley. The compensation force is generated by the gravity of the counterweight and transmitted through the cable and pulley to the force adjuster. The force generated by the counterweight can be modeled as

$$F_c = m_c g + m_c a_c, \tag{4}$$

where m_c is the mass of the counterweight and a_c is its acceleration. The constant force spring design comprises two constant springs, a prismatic sliding guide, and a cart. Two constant force springs are fixed on the guide and connected in parallel to one end of the cart that can move freely along the guide to form a combined force to pull the cart. The other end of the cart is connected to the force adjuster via a cable. The force generated by the constant force spring can be expressed as

$$F_c = 2F_s, \tag{5}$$

where F_s is the constant force of each spring.

The counterweight design introduces additional inertia into the system, potentially adversely affecting dynamics during fast motion. However, it offers simplicity and reliability, with the weight of the counterweight easily adjustable. On the other hand, the constant force spring solution avoids introducing additional weight (assuming the mass of the cart is negligible) and provides a constant compensating force. However, this design is associated with drawbacks, including a more complex installation and fixation design, the friction generated by the sliding guide that gradually increases with use, and the limited selection of constant force springs which complicates the adjustment of the output force.

The force adjuster, as depicted in Fig. 6c, is primarily devised for situations where the applied force cannot be arbitrarily changed, such as the weight of the counterweight or the tension of the spring. It constitutes a fixed combination of a standard pulley and a conical pulley. The conical pulley can continuously vary the wrapping radius by sliding the pulley sockets through a set of worm gears. This mechanism allows for changing the force arm and adjusting the final output compensation force. The force finally exerted on the platform is

$$F_t = \frac{r_c F_c}{r_t}. \tag{6}$$

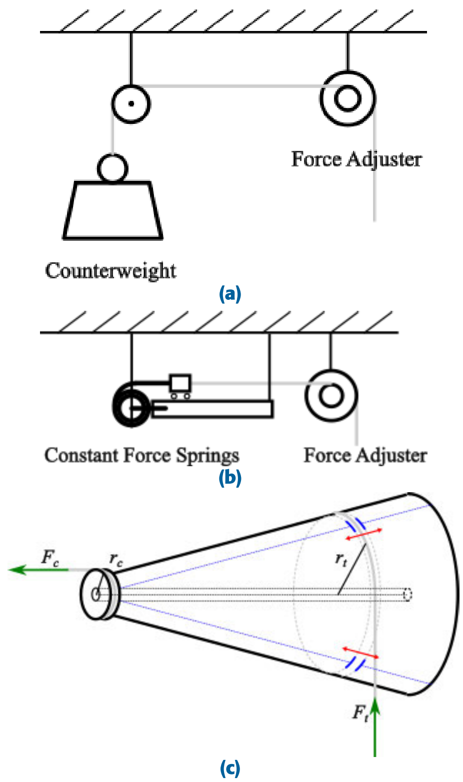

FIGURE 6. a) The counterweight solution utilizes a counterweight and a pulley, with a cable attached to the weight and connected to the force adjustor. b) In the constant force spring solution, two constant force springs are fixed at one end of the sliding guide rail and connected to a sliding cart that can move along the guide rail. A cable is tied to the other end of the cart to output the force. c) Force adjuster presents a conical design. At the top of the cone is a pulley connected to the force generator. Three worm gears are on the cone parallel to its surface and symmetrically distributed with its central axis, mounted with three pulley seats that can traverse and together form a larger pulley with an adjustable radius.

B. ELECTRONICS, SENSORS, AND COMMUNICATION

The aerial platform is equipped with two onboard computational units. The fore is an *Intel NUC7 i7 BNH* with Linux and Robotic Operating System (ROS). It is addressed to command the system and interface with the ground teleoperation computers. The latter is a *DJI A3 Pro Flight Controller* that manages the signals coming from the first computer and produces the related commands on the rotors. The ground control station (GCS) comprises a Dell Alienware laptop and a set of *Oculus Rift S* VR user interfaces.

On the platform, each arm consists of three custom electronic cards that command the six motors, including one DCX22S-12V motor with GPX22 83:1 gearbox for the shoulder actuation, four DCX22s-24V motors with customized 204.8:1 gearbox for the elbow actuation and one DCX16S-12V motor with GPX10 111:1 gearbox for the wrist actuation. The VSA-Cubes of the head use one independent electronic card. Low-level motor position control has been implemented and integrated into the electronics, and a more detailed description can be found in [32]. The hands rely on their integrated electronics, with a more detailed description in [26].

Six 24 V batteries (DJI TB47S) power the DJI aircraft in 3*P*2*S* configuration and provide power outputs at 48V, 24V, and 18V. The 48V source is responsible for powering the propellers, while the 24V is dedicated to supplying power to the arms and the head in parallel through three independent chains. Additionally, the 18V source is utilized to power the onboard computer.

The aerial platform possesses three *D-RTK GNSS*, which are high-precision navigation and positioning systems that provide an accurate, centimeter-level 3D positioning in outdoor environments. It is also capable of withstanding magnetic interference. Moreover, the Zed Mini Stereo Camera (Fig. 5) embedded in the head provides the operators with visual feedback on the workspace.

The data channels of the head and arms electronics are coupled in a series and connected to the first computer via a serial port. The stereo camera is connected to the onboard computer through an independent USB 3.0 port. A dedicated system ensures bilateral communication between the GCS and the aerial platform. The communication channel consists of a 5GHz wireless connection using a Wi-Fi bridge, which allows the exchange of control and vision data. However, a 5G internet key can achieve the same result, eliminating the necessity of flying near the Wi-Fi router. The framework is similar to the one employed in a previous work [28], and we refer to it for additional details.

IV. SYSTEM MODEL

A. KINEMATICS

To describe the suspended aerial manipulator model from a kinematic and dynamic point of view, we consider the carrying structure to be fixed, and therefore, the suspension point is considered stationary.

Define $\{I\}$ as the inertial frame attached to it, and $\{B\}$ as the frame attached to the body with the origin located at the geometric center O' of the vehicle (shown in fig. 7a). The first and second axes of the body-fixed frame lie in a common plane defined by the six rotors, pointing forward and leftward, and the third axis is orthogonal to the plane, pointing upward of the platform.

The kinematic model of the system can be considered as a floating base mobile robot described by

$$q = \begin{bmatrix} q_{fb} \\ q_{lb} \end{bmatrix}, \tag{7}$$

where $q_{fb} \in \mathbb{R}^6$ is the configuration of the floating base and $q_{lb} \in \mathbb{R}^{12}$ is the configuration of the humanoid manipulator.

We define the configuration q_{fb} of the floating base as a combination of the position of the $\{B\}$ frame origin expressed in $\{I\}$, denoted as $p = \begin{bmatrix} p_x & p_y & p_z \end{bmatrix}^T$, together with the rotation of $\{B\}$ with respect to $\{I\}$, described by Euler angles

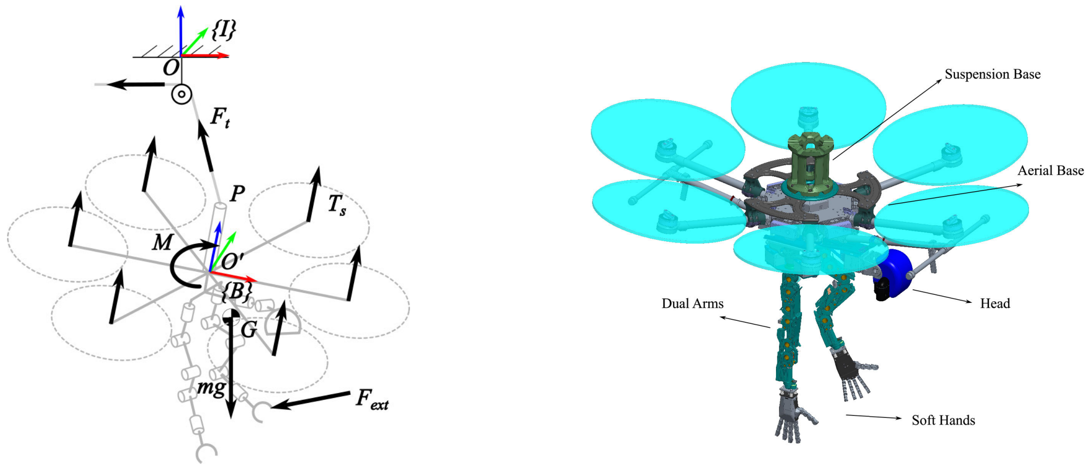

FIGURE 7. **a) System model that specifies the inertial frame and the body frame. b) Visualization of the humanoid design of the aerial manipulator.**

$\Phi = \left[\phi \ \theta \ \psi\right]^T$. That is

$$q_{fb} = \begin{bmatrix} p \\ \Phi \end{bmatrix}. \tag{8}$$

The configuration of the humanoid manipulator $q_{lb} \in \mathbb{R}^{12}$ is composed of three parts

$$q_{lb} = \begin{bmatrix} q_{la} \\ q_{ra} \\ q_h \end{bmatrix}, \tag{9}$$

where $q_{la} \in \mathbb{R}^5$ and $q_{ra} \in \mathbb{R}^5$ represent the joint variables of the 5-DoF left and right arms, $q_h \in \mathbb{R}^2$ represents the joint variables of the 2-DoF head.

B. DYNAMICS

Let m_i be the mass of the i-th humanoid torso component, m_{fb}, and m_{rod} be the mass of the drone and the suspension base attached to the drone. The total mass of the system m is

$$m = m_{fb} + m_{rod} + \sum m_i. \tag{10}$$

The position of the CoM of the humanoid torso components can be obtained from direct kinematics and is dependent on the current humanoid configuration q_{lb}. Defined c as the CoM vector of the whole body expressed in the body frame, it holds

$$c(q_{lb}) = \frac{1}{m}(m_{fb}p_{fb} + m_{rod}p_{rod} + \sum m_i p_i(q_{lb})). \tag{11}$$

Similarly, the inertial tensor of the platform expressed in the body frame relative to the origin O' can be written as

$$I_{O'}(q_{lb}) = I_{fb} + I_{rod} + \sum I_i(q_{lb}). \tag{12}$$

Due to the coupling effect between the aerial platform and the robotic arm, the complete dynamics of the system pose a complex challenge, especially during rapid movements of the robotic arms. However, serving as an aerial human-operated avatar working in unknown and unstructured work scenarios, rapid arm movements are not part of the design intent of the platform. Firstly, rapid arm motion will increase the possibility of accidental collision between the platform and the unknown external environment. Secondly, it will also increase the interference of the fuselage movement on the UAV, thereby reducing its overall stability. Considering the two points above, employing slow arm motion represents a pragmatic approach to address this problem. Under the assumption that the robotic arms move at a relatively slow pace, the system dynamics can be simplified as that of a rigid body, allowing for the neglect of coupling effects for practical considerations. This simplification facilitates a more manageable analysis and control of the system.

We can express the dynamics of the body frame as

$$\begin{bmatrix} F \\ \tau_{O'} \end{bmatrix} = \begin{bmatrix} mI_3 & -mS(c) \\ mS(c) & I_{O'} \end{bmatrix} \cdot \begin{bmatrix} \ddot{p} \\ \dot{\omega} \end{bmatrix} + \begin{bmatrix} -mS^T(\omega)S(\omega)c \\ S(\omega)I_{O'}\omega \end{bmatrix}, \tag{13}$$

where F is the force and $\tau_{O'}$ is the torque applied to the body center O', $S(\cdot)$ is the skew-symmetric matrix operator, $\omega \in \mathbb{R}^3$ is the angular velocity expressed in the body frame. Let $R \in SO(3)$ be the rotation matrix of the body-fixed frame with respect to the inertial frame; there is

$$\dot{R} = RS(\omega). \tag{14}$$

Assuming $T_s \in \mathbb{R}$ to be the total thrust and $M \in \mathbb{R}^3$ the total moment generated by the hexacopter motors and taking into account the known compensating force F_t introduced by the tether, F_{ext} is the external force applied to the manipulator and τ_{ext} is its torque to the body center, the force and torque applied to the body frame are

$$F = T_s Re_3 + F_t - mge_3 + F_{ext}, \tag{15a}$$
$$\tau_{O'} = M + S(le_3)R^T F_t - S(c)R^T mge_3 + \tau_{ext}, \tag{15b}$$

where $e_3 = \left[0 \ 0 \ 1\right]^T$, and l is the distance from the cable attached point to the origin of the body-fixed frame.

V. CONTROL STRUCTURE

The control framework of the aerial platform includes the control system and the teleoperation user interface.

A. CONTROL SYSTEM

The control system is divided into three parts, respectively the aerial base, the dual robotic arms, and the head.

1) AERIAL BASE

The primary control objective for the aerial base is to sustain its position and attitude stability while mitigating interference induced by arm motion and contact when the humanoid torso manipulates. Substituting (15) into (13), six equations arise with six variables, namely $T_s \in \mathbb{R}$, $M \in \mathbb{R}^3$, and a two-dimensional direction of F_t with a known absolute value. Given the external force F_{ext} and its torque τ_{ext}, a solution to the dynamic equations consistently exists to uphold the equilibrium of the system.

To initiate the analysis, we consider the external force as a disturbance and concentrate on a configuration where the aerial platform stabilizes at a specific position while maintaining a zero attitude. This configuration is characterized by $p = 0$, $\dot{p} = 0$, $\Phi = 0$, and $\dot{\Phi} = 0$, signifying that the translational velocity, roll angle, and roll rate of the platform are all zero. This configuration is optimal for various operational scenarios and warrants special attention due to its unique characteristics.

It is known that under small angle assumption, there is $\omega \approx \dot{\Phi} = 0$. In the neighborhood of this equilibrium, the Coriolis term can be neglected, and the dynamic equations in (13) can be written as

$$T_s e_3 + F_t - mge_3 = m\ddot{p} - mS(c)\dot{\omega}, \tag{16a}$$
$$M - S(c)mge_3 = mS(c)\ddot{p} + I_{O'}\dot{\omega}. \tag{16b}$$

In the equilibrium, it holds

$$\bar{T}_s e_3 + F_t - mge_3 = 0, \tag{17a}$$
$$\bar{M} - S(c)mge_3 = 0. \tag{17b}$$

Assuming $T_{s_d} = \bar{T}_s + \delta T_s$ and $M_d = \bar{M} + \delta M$ to be the desired total pulling force and total moment generated by the thrusters, substituting it to (16) and (17), the incremental dynamic equations can be obtained

$$\delta T_s e_3 = m\ddot{p} - mS(c)\dot{\omega}, \tag{18a}$$
$$\delta M = mS(c)\ddot{p} + I_{O'}\dot{\omega}. \tag{18b}$$

In the context of an under-actuated UAV employing parallel thrusters, it is widely recognized that the translation dynamics associated with the x and y directions are coupled with its pitch and roll dynamics. However, the yaw dynamics can be treated as decoupled from the other aspects, and controlling yaw holds a distinct priority [21], [33]. Consider the decomposition of (18a) along z axis, the altitude dynamic can be decoupled as

$$\delta T_s = m\ddot{p}_z. \tag{19}$$

It can be derived from (16a) that p_x and p_y will converge to zero when pitch and roll are stabilized due to the suspending force F_t. Thus we ignore the translation coupling term in (18b) when considering the rotation control. We expect that the behavior of the system with respect to altitude and attitude manifests in a second-order form, as outlined below

$$\ddot{p}_z + b_1\dot{p}_z + k_1(p_z - p_{z_d}) = 0, \tag{20a}$$
$$\dot{\omega} + B_2\dot{\Phi} + K_2(\Phi - \Phi_d) = 0. \tag{20b}$$

The control law is designed as

$$T_{s_d} = mg - F_t + m(-b_1\dot{p}_z - k_1(p_z - p_{z_d})), \tag{21a}$$
$$M_d = S(c)mge_3 + I_{O'}(-B_2\dot{\Phi} - K_2(\Phi - \Phi_d)), \tag{21b}$$

where p_{z_d} is the reference altitude, and Φ_d is the reference attitude input by a motion planner receiving user commands.

For common commercial UAV platforms with non-open autopilots, such as DJI, access to the control of individual motors is typically restricted. Instead, attitude control is usually achieved through a built-in attitude controller, utilizing the total pulling force of the motor T_{s_d} and the desired attitude angle Φ_d or angular velocity $\dot{\Phi}_d$. Consequently, the proposed approach, involving the output of desired T_{s_d} and M_d, cannot be directly implemented but serves as an outer loop connected to the built-in attitude controller. The built-in attitude controller is assumed to be based on the classic model-independent PD control law, as presented in [34]. In angular velocity control mode, the relationship between angular velocity command $\dot{\Phi}_d$ and the generated torque $\hat{M}$ can be written as:

$$\hat{M} = b_\Phi(\dot{\Phi}_d - \dot{\Phi}). \tag{22}$$

Substituting $\hat{M}$ with the M_d in (21), the outer loop control output is expressed as

$$T_{s_d} = mg - F_t + m(-b_1\dot{p}_z - k_1(p_z - p_{z_d})), \tag{23a}$$
$$\dot{\Phi}_d = \frac{S(c)mge_3 + I_{O'}(-B_2\dot{\Phi} - K_2(\Phi - \Phi_d))}{b_\Phi} + \dot{\Phi}. \tag{23b}$$

2) DUAL ARMS

The control of the arms is divided into two parts. The first computes the position of the joints to obtain the tracking of the reference trajectory. The latter computes the necessary conversion from the joint angles to the motor routing derived from the tendons structure.

The joint position is calculated through a weighted inverse kinematic algorithm [35]. The desired joint velocities vector of the arm $\dot{q}_{a_d}$ ($\dot{q}_{ra_d}$ for the right arm or $\dot{q}_{la_d}$ for the left) can be computed by

$$\dot{q}_{a_d} = J_w^\dagger K(x_d - x_e), \tag{24}$$

where K is a diagonal coefficient matrix, x_d is the desired end-effector position given by user joysticks, and x_e is the actual end-effector position calculated using direct kinematics. The matrix $J_w^{\dagger}$ is the weighted pseudo-inverse of the Jacobian matrix J:

$$J_w^{\dagger} = W^{-1}J^T(JW^{-1}J^T)^{-1}, \tag{25}$$

where W is a symmetric positive definite weight matrix used to optimize the controller performance when the arms are close to a kinematic singularity. The desired joint variable vector q_{a_d} is calculated using an integration performed in discrete time with numerical techniques:

$$q_{a_d}(t_{k+1}) = q_{a_d}(t_k) + \dot{q}_{a_d}(t_k)\Delta t. \tag{26}$$

The desired motor position command q_{m_d} is obtained from the desired joint variable using the previously specified relationship between joints and tendons:

$$q_{m_d} = F^{\dagger} q_{a_d}, \tag{27}$$

where $F^{\dagger}$ is the pseudo-inverse of the configuration matrix F. The command q_{m_d} is used as the reference input of the position servo motor and is executed by the lower-level motor driver.

3) NECK AND HEAD

The head controller employs an inverse kinematics algorithm similar to that of the arm. The expected joint variables are calculated using the desired head position from the Oculus headset orientation. Since the motors straight actuate the neck joints, the computed joint variables are directly used as the motor references.

B. TELEOPERATION

The teleoperation system is implemented using the GCS introduced in Section III-B. This GCS incorporates an immersive VR headset for first-person perspective visualization and head orientation tracking, along with two joysticks for user command input.

The sensing and control mechanisms within the teleoperation framework are designed for real-time operation. Following the capture of the raw image by the stereo camera, it is promptly transmitted to the VR headset, providing the operator with a first-person perspective of the field of view of the camera. The human operator's movements, tracked through the headset and two handheld joysticks, are transformed from the Oculus coordinate into the platform body coordinate in real time. These transformed movements are then employed as the reference input for the robot head and arm control system. The thumbsticks of both joysticks are utilized to command the movement of the aerial base. Specifically, the left-hand thumbstick adjusts the desired altitude, while the right-hand thumbstick gives yaw rotation commands. The trigger on each joystick controls the closure of the corresponding robotic hand.

Fig. 8 shows the control framework. The GCS software is implemented using Oculus SDK with a ROS node. The control algorithms presented in V-A are also implemented with ROS and run on the onboard computer. The inputs to the

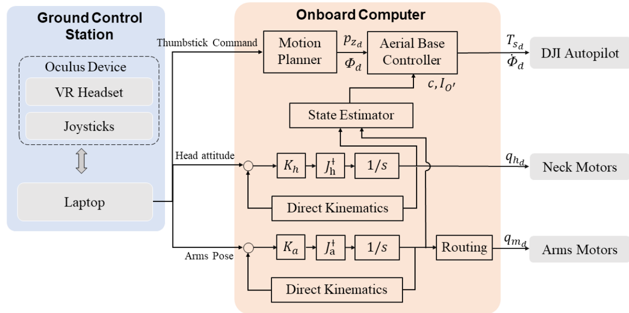

FIGURE 8. Control framework. On the left is the teleoperation user interface described in V-B, in the middle is the control system described in V-A running on the onboard computer, and on the right is the low-level controller described in III-B.

onboard control system consist of the thumbstick commands, the arm position and orientation reference trajectory, and the head orientation reference. The output aerial base commands are transmitted to the A3 Pro Flight Controller via a predefined communication protocol in the DJI onboard software development kit. Arm and neck commands are simultaneously sent to their driver boards.

VI. EXPERIMENTAL VALIDATION AND RESULTS

The effectiveness of the aerial platform has been validated through two types of experiments. The performance of the aerial base stabilization control described in Sec. V is evaluated by varying the CoM of the system through a series of body movements. The capabilities of the design are demonstrated through a sequence of tasks to relight light bulbs in a disaster response scenario reproduced under laboratory conditions.

A. SETUP

For safety reasons, all of the experiments were conducted indoors under the protection of a test rig setup. An Optitrack infrared motion capture system was used to provide information for state estimation to restore the outdoor situation where RTK is available. Fig. 9 shows the experiment setup.

The test rig incorporates gravity compensation as described in Sec. III, while limiting the space available for movement of the aerial platform to prevent accidents during flight testing that could cause damage to humans or the system itself. The test rig consists of three main parts. The first part is the support structure that holds the entire rig frame to the ceiling. The second part is a frame constructed from two coaxial parallel rings fixed to the first part. It defines a cylindrical movable space for the platform and creates setbacks in roll and pitch angles and radial displacement. The third part is a rod-like structure solidly attached to the hexacopter aerial base, adding a weight of $m_{rod} \approx 7$ kg to the main part of the platform of $m_{fb} + \sum m_i \approx 17$ kg. Its upper tip passes through the ring of the second part and restricts the movement of the aerial base in the vertical direction by means of two disks attached to the rod. The combination of

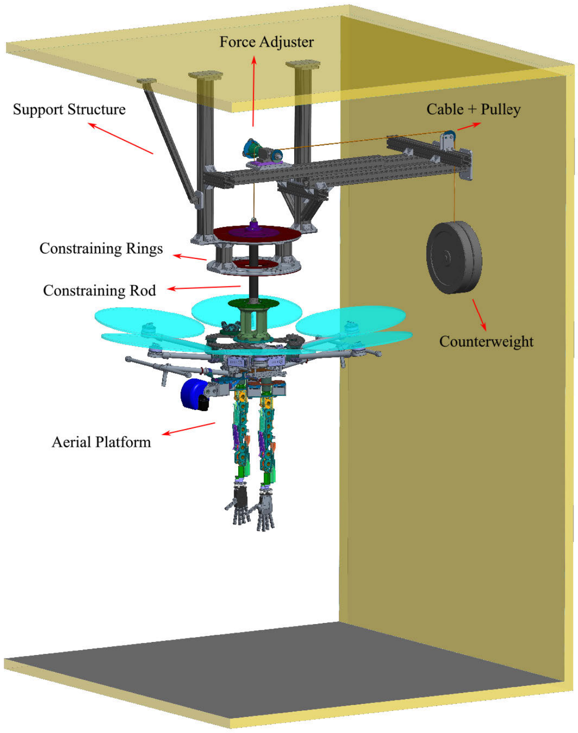

FIGURE 9. Experiment setup. The aerial platform is suspended by a cable and pulleys, with a counterweight on the other end that partially compensates for its gravity. A test rig attached to the ceiling and the wall constrains the movement of the aerial platform from accidental collision, described in detail in VI-A.

the constraining components creates an activity space that allows the platform to translate within a cylindrical space with radius $r \approx 4.7$ cm and height $h \approx 17$ cm, while allowing a rotation of up to $\Delta\phi = \Delta\theta \approx \pm 30°$ for pitch and roll. More details about the design of the test rig can be found in [36].

The two gravity compensation schemes based on counterweights and springs mentioned in Sec. III-A were implemented. In the following indoor experiments, the counterweight design was deployed. A 15 kg counterweight was used as the force generator, and the force adjuster ratio was set to 1:1. Considering that the total weight of the aerial manipulator connected to the tether is approximately 24 kg and the tether is configured to compensate for 15 kg, the aerial base still needs to generate 9 kg of thrust, which is 27% of its maximum load capacity. The designed compensating force aims to keep the thrust at a value slightly lower than the nominal state of the hexacopter to reduce the energy consumption of the aerial system. We chose not to compensate for all of the force to prevent the capabilities of the platform to generate rotational torque from declining too much due to insufficient thrust. In all designed experiments, the aerial platform does not involve rapid motion, and the impact of the additional inertia brought by the counterweight on the system is negligible. Therefore, the compensation force is approximated by the weight of the counterweight $F_t \approx m_c g$, which can be validated by the posterior experimental data (in normal working conditions, $|a_c| < 0.7\text{m/s}^2 \ll g$).

B. CONTROL VALIDATION

To validate the effectiveness of the proposed control in stabilizing attitude, we conducted two experiments to compare the control performance with and without the proposed aerial base outer loop control in a disturbance rejection task.

As mentioned above, the DJI autopilot requires additional sensor support for hovering in an indoor scenario. Therefore, the altitude and yaw control of the aerial base described by (23) was facilitated to keep the aerial manipulator hovering in both of the two experiments, wherein Optitrack feedback was employed. The joints of the arms are systematically controlled following a predetermined motion sequence to induce disturbances in the system. The fundamental distinction between the two experiments lay in the control of roll and pitch. In one experiment, solely the DJI built-in attitude controller was utilized with zero as the input for roll and pitch control. In the other experiment, the proposed outer loop control was applied for roll and pitch. The uniform objective remained consistent with stabilizing body attitude angles Φ at the zero position. This goal served as the benchmark for evaluating the performance of the proposed controller in mitigating disturbances induced by CoM shifting and effectively stabilizing the desired attitude.

The results are shown in Fig. 10. An estimate of the overall CoM shift caused by the movement of the robotic arms is illustrated in the figure. It can be seen (left column of Fig. 10) that the larger CoM variation happens along the x direction of the body. From the center and right column of Fig. 10, it is possible to appreciate that applying the proposed controller can compensate for the disturbance induced on the body attitude better than with only the DJI build-in controller. The root mean square (RMS) error of the airframe attitude and position under the two controls are compared in Table 4. Along the x direction, where the disturbance is the most significant, the RMS error of the airframe attitude under the control of the proposed controller is 1.3218, compared to 2.0367 for the DJI controller.

It is observed that the oscillations in position are relatively small, on the scale of centimeters, and the differences between the experiments are not significant. This is attributed to the relatively high system stability of the tethered system. The dynamic model indicates that the position of the platform is coupled with its attitude due to the under-actuated hexacopter aerial base. When the suspension point is stationary, the position deviation tends to converge to zero as the attitude converges to zero. However, if the suspension point moves, the dynamics will differ, requiring further analysis. Nonetheless, this situation involves the motion of the carriers and is beyond the scope of this paper.

C. TASKS VALIDATION

The capacity of aerial manipulators for flight confers the distinct advantage of disregarding ground-level debris

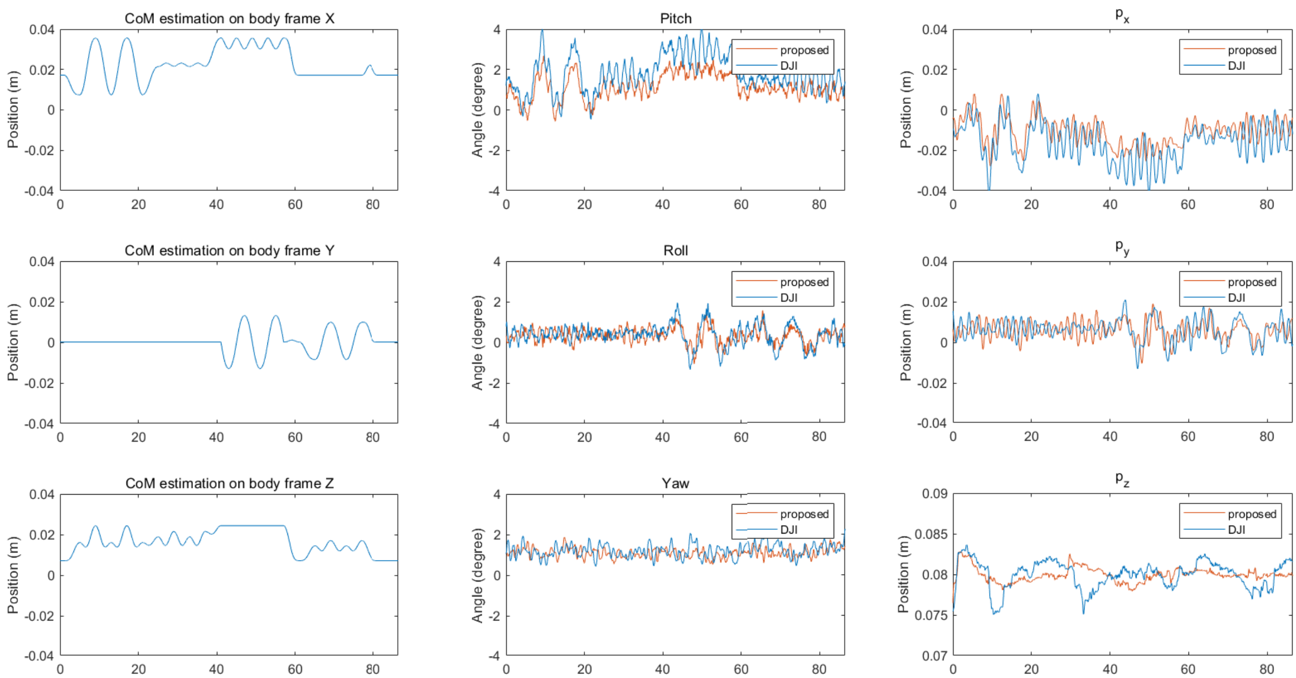

FIGURE 10. Plots of control validation experiment result, the response of the two controllers to a test shift in the center of mass position (left column). Pitch, Roll, and Yaw (central column) and p_x, p_y and p_z positions of the body frame (right column). The results of the DJI built-in controller are in blue, and those of the proposed control are in red.

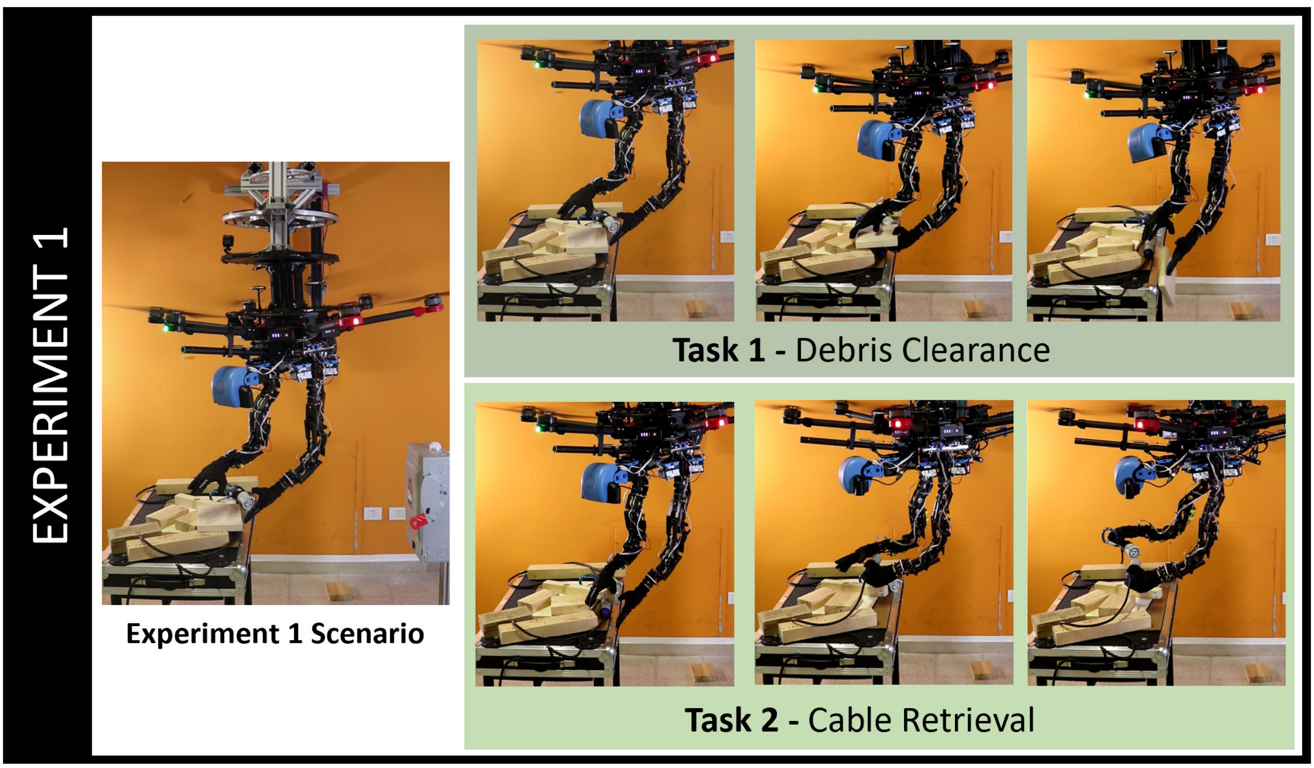

FIGURE 11. Photo sequence of the first experiment scenario as described in VI-C, in which the aerial platform sequentially performed two tasks: Debris clearance and cable retrieval. The platform first picked up and removed a wooden brick to reveal the buried aviation connector. Then, it used two hands to pick up the two connectors, one in each hand.

and obstacles, rendering them particularly well-suited for applications in post-disaster scenarios.

To substantiate the overall functionality of the proposed aerial platform, we designed a scenario simulating a

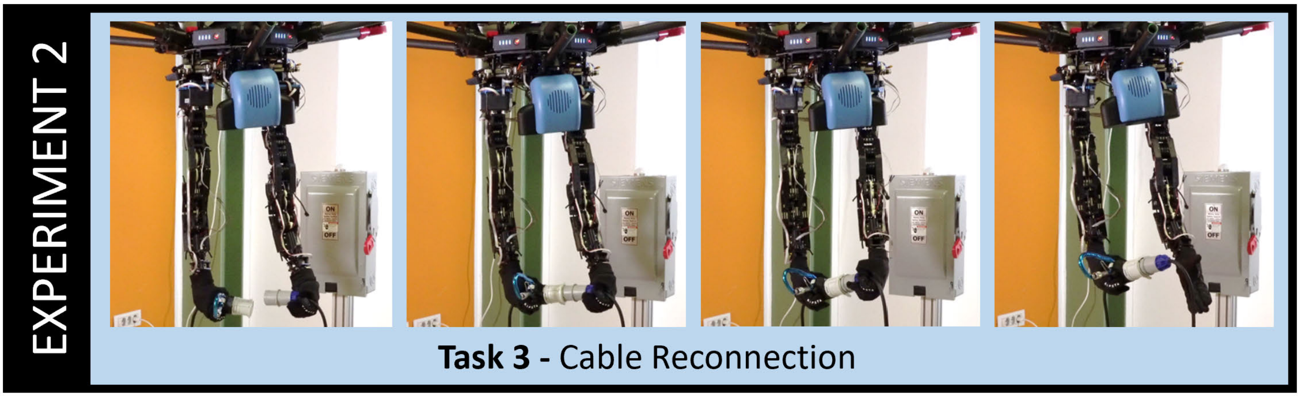

FIGURE 12. Photo sequence of the second experiment of cable reconnection as described in VI-C. The aerial platform used both hands to collaboratively insert the connector it grabbed in the previous scenario.

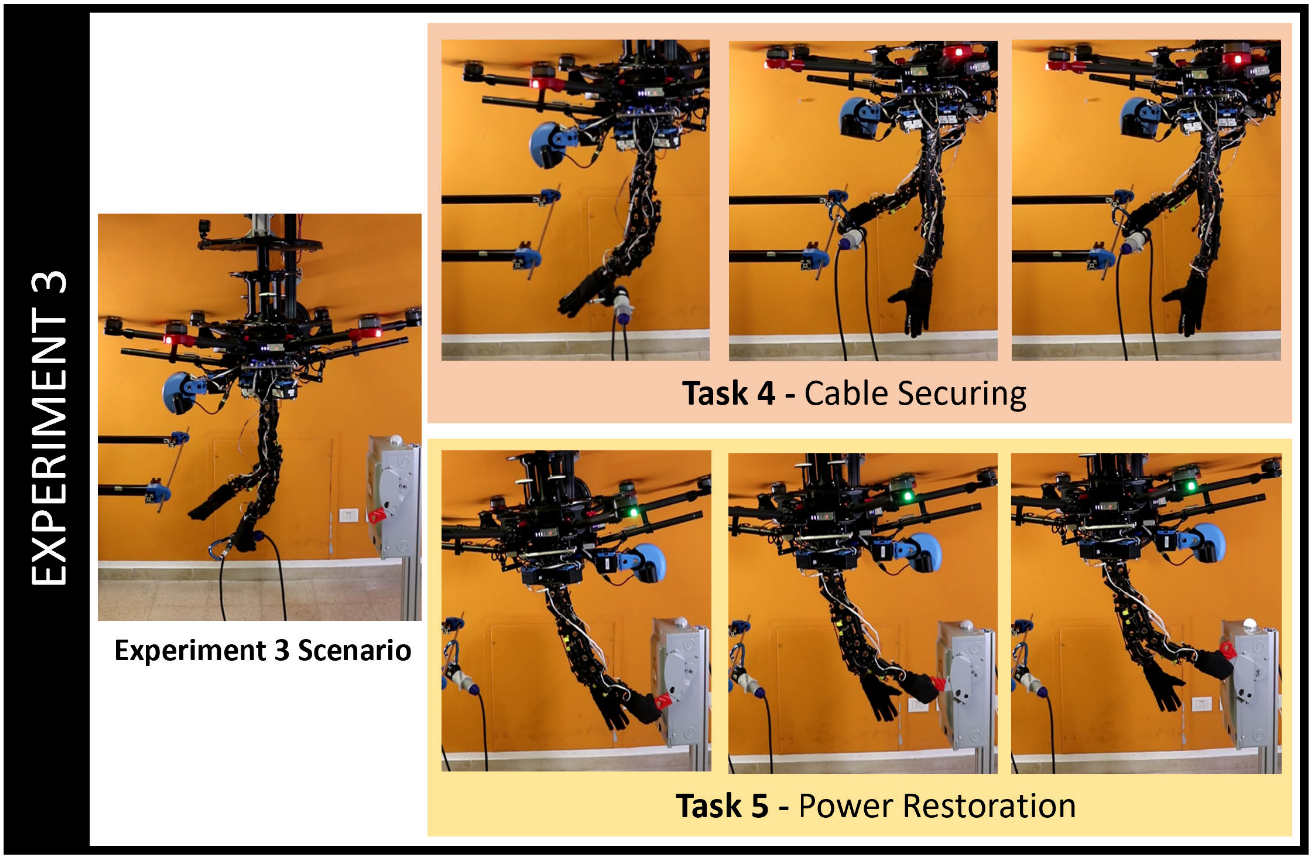

FIGURE 13. Photo sequence of the third experiment scenario as described in VI-C, in which the aerial platform sequentially performed cable securing and power restoration. It first switched the connected connector from the left hand to the right hand, raised the height, and snapped the spring hook attached to the connector onto the crossbar. Then, it turned backward and lifted the switch up to light the bulb.

TABLE 4. Performance comparison between proposed control versus DJI built-in control.

RMS errors	Rotation($^\circ$)			Position(m)		
	θ	ϕ	ψ	p_x	p_y	p_z
DJI	2.0367	0.6338	1.2343	0.0190	0.0082	0.0800
proposed	1.3218	0.4986	1.1114	0.0130	0.0074	0.0799

post-disaster situation. In this scenario, a severely damaged building has experienced a disruption in its internal power and communication cables. To facilitate rescue and reconstruction, robots are required to access the building, re-establish the cable connections, and restore power. To facilitate systematic reproduction and analysis within a laboratory setting, we divided the workflow into five tasks:

- Debris Clearance: The initial phase involves the clearance of debris at the site to locate the disconnected cables efficiently.
- Cable Retrieval: The disconnected cables must be gathered for further handling.

- Cable Reconnection: Following collection, the cables need to be skillfully reconnected, necessitating the use of both hands.
- Cable Securing: To mitigate the risk of short circuits due to potential ground-level water exposure, the cables must be elevated to a higher level by a hook.
- Power Restoration: The process culminates in the restoration of power through the activation of a switch.

Due to the limitations of the movement space and safety considerations, these five steps could not be accomplished in a single session, so we performed the five tasks in three scenarios. In the experiments, wood bricks of different sizes and shapes on a table were used to represent debris on the ground. A common electric box and a cable connected to industrial aviation connectors with a typical spring hook attached were also used. All the experiments were performed with the control methods described in Sec. V and were teleoperated remotely by a human operator located in another room.

a: DEBRIS CLEARANCE (1) AND CABLE RETRIEVAL (2)

Fig. 11 shows the first two tasks completed consecutively in one experiment. In the experimental scenario, wooden bricks of diverse sizes and shapes were arranged in a random manner on a table to replicate the appearance of scattered debris. Concealed beneath the simulated debris was a cable equipped with industrial aviation connectors. At the beginning of the task, the platform looked around to locate the connectors. Subsequently, the manipulators engaged in the retrieval and removal of the debris covering the connectors. Following this, it employed each of its hands to grasp the exposed connectors.

This experiment demonstrates the grasping ability of the proposed aerial platform for objects of different sizes and shapes. The presence of SoftHands enables the platform to manipulate irregularly shaped objects. It is worth mentioning that during the grasping process, the arm unavoidably came into contact with the tabletop and exerted a force. The flexible joints successfully mitigated the impact forces during the contact, and the controller resisted this disturbance and smoothed the body attitude.

b: CABLE RECONNECTION (3)

In order to provide a clearer visual representation of this procedure, we removed the table used in the preceding experiment to create the necessary space. Fig. 12 presents the process of connecting the grasped aviation connectors. Alignment and splicing is a challenging task that requires two-handed collaboration to accomplish. The arm dexterity and bi-manual manipulation ability are demonstrated in this task.

c: CABLE SECURING (4) AND POWER RESTORATION (5)

Fig. 13 introduces the last two tasks performed consecutively. The aerial platform was initiated by grasping the connected connectors with its left hand, subsequently transitioning to the spring hook onto its right hand. Following this, it elevated the assembly to the desired height and engaged the spring hook onto a beam structure. Subsequently, it executed a 180-degree rotation and proceeded to vertically actuate the switch, ultimately lighting the bulb.

In a more coordinated motion to lift the switch, the operator elevated the height of the aerial base while simultaneously lifting the arm, effectively leveraging the freedom of movement of the aerial base as retained in our design. The compliance of the arms played a crucial role in successfully executing this task during the procedure. It is noteworthy that during the initial attempt to lift, the hand grasp was not positioned correctly, resulting in the finger getting caught in the switch. To free the hand from the switch, the arm had to apply a substantial force, consequently producing a significant disturbance on the body. However, the flexible joint design preserved the integrity of the arms, and the proposed controller ultimately stabilized the body.

D. DISCUSSION

The experimental results demonstrate the effectiveness of the system in environments that are challenging to access from the ground. It exhibits the necessary dexterity to handle tasks involving different targets, adaptively manipulating objects of varying shapes and sizes. The proposed control and teleoperation framework effectively maintains body stability in flight, demonstrating robustness to disturbances. Simultaneously, it allows the operator to safely and intuitively engage in various tasks involving physical interaction with the external environment.

Furthermore, experiments (4) and (5) showcased the system manipulation capabilities in a cable suspension working environment, illustrating ascent, descent, and rotation capabilities. The manipulation workspace was successfully demonstrated within the constraints of the test rig, suggesting the potential for further expansion beyond these limitations, particularly with the utilization of a movable suspension base, such as a crane.

1) LIMITATIONS AND FUTURE WORK

The choice of the DJI M600 Pro as the aerial base is driven by its sufficient drive capabilities. However, it is essential to note that its powerful downwash airflow can pose challenges when dealing with lighter objects such as paper, making their operation difficult. In light of this, there is a willingness to explore different possibilities by considering the use of alternative multirotors, potentially smaller ones. An investigation into the advantages and limitations of these alternatives will be a focus of further research. While the tendon transmission design of the arm offers improved weight distribution and compliance, it does come with a trade-off in terms of lower end-effector positioning accuracy compared to direct transmission. However, this deviation can be easily compensated for by human operators during teleoperation, highlighting the adaptability of first-person perspective operation.

The proposed controller exhibits the capability to mitigate the effects of CoM shifts induced by arm movements and displays a degree of resilience against external forces imposed by the environment. However, it has some limitations: the controller is based on a simplified model, where the reaction torque caused by whole-body motion is not fully considered; during the linearization process, the designed controller primarily focuses on balancing the system at the zero attitude, which treats the external force as a disturbance and does not take its control into account. These limitations bring some problems: when the aerial platform performs fast limb movements or encounters large external disturbances, the performance of the proposed controller becomes compromised. For example, experimental observations show that under a huge external disturbance, the system may not revert to the initial attitude but instead stabilize at a non-zero attitude. This phenomenon may be attributed to inherent nonlinearities within the system or other unmodeled phenomena, possibly arising inside the closed DJI hexacopter controller or the unmodeled external force, necessitating further in-depth analysis. Therefore, our further research aims to enhance its capability and robustness under such conditions, requiring a more complex whole-body nonlinear controller. In the future, the applied force will be further included in the control, for which force estimation may also need to be considered.

In the designed working scenarios of the robot platform, such as post-earthquake ruins, visibility is frequently limited, posing challenges for observation through optical cameras alone. As part of our future work, we are contemplating the simultaneous integration of additional sensors, such as ultrasound or LiDAR, to augment the visual feedback. Besides, one of the main factors that affect the operational effectiveness lies in the absence of haptic sensors and force sensors. Relying solely on visual information hinders the intuitive perception of the state of the operating object. This limitation sometimes leads to misjudgments in the operational process, resulting in operational failures. Thus, we plan to integrate haptic sensors and force estimation into teleoperation in the future. This multi-sensor approach aims to enhance the perception capabilities, enabling more effective operation in challenging conditions. Furthermore, it is pertinent to note that the transmission delay for control instructions remains minimal, ranging from 10ms to 100ms. In contrast, the video stream encounters more significant delays due to data compression and processing, typically averaging around 1s depending on the network connection. While the delay in the arm control is negligible, the video stream delay is crucial as operators depend on visual feedback from the robot camera to execute subsequent actions. A notable video delay could hinder the operator's reaction time and operational efficiency to some extent. However, advancements in communication technology offer potential avenues for improvement in this regard.

VII. CONCLUSION

In this paper, we presented a novel Suspended Aerial Manipulation Avatar prototype. It comprises a hexacopter aerial base and a humanoid torso together with a variable-length suspension system, and is capable of safely executing various interactive tasks in unknown environments. In comparison to existing solutions, our approach offers an advantage by preserving the freedom of motion for the aerial base while utilizing variable-length cable suspension to extend flight duration. Furthermore, concerning the design of the aerial base, our solution is universal as it can be integrated with commercial UAVs instead of necessitating a dedicated design. A stabilizing control that considers the humanoid torso motion and the role of the tethering system, complemented by an immersive teleoperation framework was presented. The SAM-A prototype and the proposed control were demonstrated in experiments, highlighting its strengths and weaknesses.

Our further research will focus on a more comprehensive nonlinear whole-body controller to explore the potential of the platform. Future investigations will also explore the application of the aerial platform in field-like experiments, where the aerial manipulation avatar could operate attached to a large crane and/or in free-flight mode. Moreover, we will investigate the deployment of autonomous operation modes on the aerial platform to assist and simplify teleoperation, as well as further achieve full autonomous control.

ACKNOWLEDGMENT

The authors would like to thank Giacomo Dinuzzi and Manuel Barbarossa for their help with the arm design; Andrea Di Basco, Vinicio Tincani, Mattia Poggiani, and Cristiano Petrocelli for their valuable support in the development of the hardware prototypes; and Andrea Cavaliere and Federica Barontini for their assistance in the experimental validation.

REFERENCES

[1] A. Ollero, G. Heredia, A. Franchi, G. Antonelli, K. Kondak, A. Sanfeliu, A. Viguria, J. R. M.-D. Dios, F. Pierri, J. Cortes, A. Santamaria-Navarro, M. A. T. Soto, R. Balachandran, J. Andrade-Cetto, and A. Rodriguez, "The AEROARMS project: Aerial robots with advanced manipulation capabilities for inspection and maintenance," *IEEE Robot. Autom. Mag.*, vol. 25, no. 4, pp. 12–23, Dec. 2018.

[2] *Aerones Drone for Wind Turbine Cleaning, De-Lcing, and Coating Applications*. Accessed: Dec. 21, 2023. [Online]. Available: https://www.youtube.com/watch?v=eBVRQDRY5mY

[3] S. Shimahara, S. Leewiwatwong, R. Ladig, and K. Shimonomura, "Aerial torsional manipulation employing multi-rotor flying robot," in *Proc. IEEE/RSJ Int. Conf. Intell. Robots Syst. (IROS)*, Oct. 2016, pp. 1595–1600.

[4] A. Ollero, M. Tognon, A. Suarez, D. Lee, and A. Franchi, "Past, present, and future of aerial robotic manipulators," *IEEE Trans. Robot.*, vol. 38, no. 1, pp. 626–645, Feb. 2022.

[5] F. Ruggiero, V. Lippiello, and A. Ollero, "Aerial manipulation: A literature review," *IEEE Robot. Autom. Lett.*, vol. 3, no. 3, pp. 1957–1964, Jul. 2018.

[6] X. Meng, Y. He, and J. Han, "Survey on aerial manipulator: System, modeling, and control," *Robotica*, vol. 38, no. 7, pp. 1288–1317, Jul. 2020.

[7] A. Suarez, A. E. Jimenez-Cano, V. M. Vega, G. Heredia, A. Rodriguez-Castaño, and A. Ollero, "Design of a lightweight dual arm system for aerial manipulation," *Mechatronics*, vol. 50, pp. 30–44, Apr. 2018.

[8] A. Suarez, G. Heredia, and A. Ollero, "Design of an anthropomorphic, compliant, and lightweight dual arm for aerial manipulation," *IEEE Access*, vol. 6, pp. 29173–29189, 2018.

[9] A. Suarez, P. J. Sanchez-Cuevas, G. Heredia, and A. Ollero, "Aerial physical interaction in grabbing conditions with lightweight and compliant dual arms," *Appl. Sci.*, vol. 10, no. 24, p. 8927, Dec. 2020. [Online]. Available: https://www.mdpi.com/2076-3417/10/24/8927

[10] M. Perez-Jimenez, P. Ramon-Soria, B. Arrue, and A. Ollero, ''Hecatonquiros: Open-source hardware for aerial manipulation applications,'' *Int. J. Adv. Robotic Syst.*, vol. 17, no. 2, Mar. 2020, Art. no. 172988142092162.

[11] P. Yang, H. Wang, Z. Liu, Z. Dong, and L. Zhang, ''Development of an anthropomorphic and dexterous dual-arm system for aerial cooperative bimanual manipulation,'' *Machines*, vol. 10, no. 4, p. 273, Apr. 2022. [Online]. Available: https://www.mdpi.com/2075-1702/10/4/273

[12] M. Orsag, C. Korpela, S. Bogdan, and P. Oh, ''Dexterous aerial robots—Mobile manipulation using unmanned aerial systems,'' *IEEE Trans. Robot.*, vol. 33, no. 6, pp. 1453–1466, Dec. 2017.

[13] C. Korpela, M. Orsag, and P. Oh, ''Towards valve turning using a dual-arm aerial manipulator,'' in *Proc. IEEE/RSJ Int. Conf. Intell. Robots Syst.*, Sep. 2014, pp. 3411–3416.

[14] (Dec. 21, 2023). *ProDrone Webpage*. [Online]. Available: https://www.prodrone.com/archives/1420/

[15] A. Suarez, A. M. Giordano, K. Kondak, G. Heredia, and A. Ollero, ''Flexible link long reach manipulator with lightweight dual arm: Soft-collision detection, reaction, and obstacle localization,'' in *Proc. IEEE Int. Conf. Soft Robot. (RoboSoft)*, Apr. 2018, pp. 406–411.

[16] A. Suarez, P. Sanchez-Cuevas, M. Fernandez, M. Perez, G. Heredia, and A. Ollero, ''Lightweight and compliant long reach aerial manipulator for inspection operations,'' in *Proc. IEEE/RSJ Int. Conf. Intell. Robots Syst. (IROS)*, Oct. 2018, pp. 6746–6752.

[17] A. Suarez, F. Real, V. M. Vega, G. Heredia, A. Rodriguez-Castaño, and A. Ollero, ''Compliant bimanual aerial manipulation: Standard and long reach configurations,'' *IEEE Access*, vol. 8, pp. 88844–88865, 2020.

[18] I. Armengol, A. Suarez, G. Heredia, and A. Ollero, ''Design, integration and testing of compliant gripper for the installation of helical bird diverters on power lines,'' in *Proc. Aerial Robot. Syst. Phys. Interacting Environ. (AIRPHARO)*. Biograd na Moru, Croatia: IEEE Press, Oct. 2021, pp. 1–8. [Online]. Available: https://ieeexplore.ieee.org/document/9571044, doi: 10.1109/AIRPHARO52252.2021.9571044.

[19] R. Miyazaki, R. Jiang, H. Paul, Y. Huang, and K. Shimonomura, ''Long-reach aerial manipulation employing wire-suspended hand with swing-suppression device,'' *IEEE Robot. Autom. Lett.*, vol. 4, no. 3, pp. 3045–3052, Jul. 2019.

[20] Y. S. Sarkisov, M. J. Kim, D. Bicego, D. Tsetserukou, C. Ott, A. Franchi, and K. Kondak, ''Development of SAM: Cable-suspended aerial manipulator,'' in *Proc. Int. Conf. Robot. Autom. (ICRA)*, May 2019, pp. 5323–5329.

[21] Y. S. Sarkisov, M. Jun Kim, A. Coelho, D. Tsetserukou, C. Ott, and K. Kondak, ''Optimal oscillation damping control of cable-suspended aerial manipulator with a single IMU sensor,'' in *Proc. IEEE Int. Conf. Robot. Autom. (ICRA)*, May 2020, pp. 5349–5355.

[22] A. Coelho, Y. Sarkisov, X. Wu, H. Mishra, H. Singh, A. Dietrich, A. Franchi, K. Kondak, and C. Ott, ''Whole-body teleoperation and shared control of redundant robots with applications to aerial manipulation,'' *J. Intell. Robotic Syst.*, vol. 102, no. 1, pp. 1–22, May 2021.

[23] J. Lee, R. Balachandran, Y. S. Sarkisov, M. De Stefano, A. Coelho, K. Shinde, M. J. Kim, R. Triebel, and K. Kondak, ''Visual-inertial telepresence for aerial manipulation,'' in *Proc. IEEE Int. Conf. Robot. Autom. (ICRA)*, May 2020, pp. 1222–1229.

[24] G. A. Yashin, D. Trinitatova, R. T. Agishev, R. Ibrahimov, and D. Tsetserukou, ''AeroVr: Virtual reality-based teleoperation with tactile feedback for aerial manipulation,'' in *Proc. 19th Int. Conf. Adv. Robot. (ICAR)*, Dec. 2019, pp. 767–772.

[25] R. Verdín, G. Ramírez, C. Rivera, and G. Flores, ''Teleoperated aerial manipulator and its avatar. Communication, system's interconnection, and virtual world,'' in *Proc. Int. Conf. Unmanned Aircr. Syst. (ICUAS)*, Jun. 2021, pp. 1488–1493.

[26] M. G. Catalano, G. Grioli, E. Farnioli, A. Serio, C. Piazza, and A. Bicchi, ''Adaptive synergies for the design and control of the Pisa/IIT SoftHand,'' *Int. J. Robot. Res.*, vol. 33, no. 5, pp. 768–782, Apr. 2014.

[27] F. Kong, S. Monteleone, G. Grioli, M. G. Catalano, and A. Bicchi, ''A robotic aerial platform with functionally anthropomorphic arms designed for physical interaction,'' in *Proc. IEEE/RSJ Int. Conf. Intell. Robots Syst. (IROS)*, Oct. 2022, pp. 7581–7588.

[28] G. Lentini, A. Settimi, D. Caporale, M. Garabini, G. Grioli, L. Pallottino, M. G. Catalano, and A. Bicchi, ''Alter-Ego: A mobile robot with a functionally anthropomorphic upper body designed for physical interaction,'' *IEEE Robot. Autom. Mag.*, vol. 26, no. 4, pp. 94–107, Dec. 2019.

[29] S. Park, Y. Jung, and J. Bae, ''An interactive and intuitive control interface for a tele-operated robot (AVATAR) system,'' *Mechatronics*, vol. 55, pp. 54–62, Nov. 2018.

[30] Y. Wang, W. Li, S. Togo, H. Yokoi, and Y. Jiang, ''Survey on main drive methods used in humanoid robotic upper limbs,'' *Cyborg Bionic Syst.*, vol. 2021, 2021, Art. no. 9817487, doi: 10.34133/2021/9817487.

[31] D. B. Camarillo, C. F. Milne, C. R. Carlson, M. R. Zinn, and J. K. Salisbury, ''Mechanics modeling of tendon-driven continuum manipulators,'' *IEEE Trans. Robot.*, vol. 24, no. 6, pp. 1262–1273, Dec. 2008.

[32] M. G. Catalano, G. Grioli, M. Garabini, F. Bonomo, M. Mancini, N. Tsagarakis, and A. Bicchi, ''VSA-CubeBot: A modular variable stiffness platform for multiple degrees of freedom robots,'' in *Proc. IEEE Int. Conf. Robot. Autom.*, May 2011, pp. 5090–5095.

[33] T. Lee, M. Leok, and N. H. McClamroch, ''Geometric tracking control of a quadrotor UAV on SE(3),'' in *Proc. 49th IEEE Conf. Decis. Control (CDC)*, Dec. 2010, pp. 5420–5425.

[34] J. T.-Y. Wen and K. Kreutz-Delgado, ''The attitude control problem,'' *IEEE Trans. Autom. Control*, vol. 36, no. 10, pp. 1148–1162, Oct. 1991.

[35] B. Siciliano, L. Sciavicco, L. Villani, and G. Oriolo, *Robotics: Modelling, Planning and Control*. London, U.K.: Springer, 2021, ch. 3.

[36] F. Kong, S. Monteleone, G. Grioli, M. G. Catalano, and A. Bicchi, ''An anthropomorphic aerial manipulator equipped with a testbed for indoor experiments,'' in *Proc. I-RIM Conf.*, 2022, Art. no. 7531248, doi: 10.5281/zenodo.7531248.

FANYI KONG (Graduate Student Member, IEEE) received the B.Eng. degree in control science and engineering and the M.Eng. degree from Harbin Institute of Technology, in 2018 and 2020, respectively. He is currently pursuing the Ph.D. degree with the Department of Information Engineering, University of Pisa. He affiliated with the Research Center ''E. Piaggio'' and in collaboration with the Istituto Italiano di Tecnologia (IIT), Genoa, Italy.

GRAZIA ZAMBELLA (Member, IEEE) received the bachelor's degree in biomedical engineering, the master's degree in robotics and automation engineering, and the Ph.D. degree in robotics and automation engineering from the University of Pisa, in 2015, 2019, and 2023, respectively. Her Ph.D. thesis was on whole-body balancing control and recovery strategies for two-wheeled and biped humanoids. During the Ph.D. degree, she collaborated with Italian Institute of Technology, Genoa, Italy, and the Research Center ''E. Piaggio,'' Pisa, Italy. She spent six months abroad with German Aerospace Center (DLR), Weßling, Germany. In 2022, she participated in the ''ANA Avatar Xprize'' Competition with the Team Alterego of Italian Institute of Technology and the University of Pisa. She is currently an University Assistant (Postdoctoral) with Technische Universität Wien, Vienna, Austria.

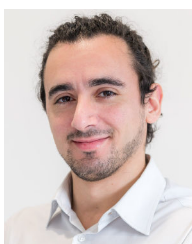

SIMONE MONTELEONE received the bachelor's degree in mechanical engineering, the master's degree in robotics and automation engineering, and the Ph.D. degree in robotics and automation engineering from the University of Pisa, in December 2015, July 2018, and July 2022, respectively. His Ph.D. thesis was on the design, control, and assessment of resilient robots. During the Ph.D. degree, he was with the Istituto Italiano di Tecnologia, Genoa, Italy, and the Research Center ''E. Piaggio,'' Pisa, Italy.

GIORGIO GRIOLI (Member, IEEE) received the Ph.D. degree in robotics, automation, and bioengineering from the University of Pisa, in 2011, with a thesis on identification for control of variable impedance actuators. Since September 2023, he has been a Senior Researcher with the University of Pisa, where he co-teaches ''robot control'' for the ''robotic and automation engineering'' master's degree course and ''automatic controls'' for the ''vehicle engineering'' master's degree course. He is the author of more than 130 scientific articles, published in scientific journals and international conference proceedings, in the fields of soft robotic actuation, robotic hand design, haptics, and human–machine interaction. He is the co-inventor of five robotic devices and helped found a spin-off company. He is a member of the Information Engineering Doctoral Board of University of Pisa, where he supervised six students and is supervising another five. He also supervised a Ph.D. student in smart industries and is supervising two Ph.D. students of national interest in robotics and intelligent machines. Over the years, he supervised the development of 40 master's theses in automation engineering and mechanical engineering courses and several bachelor's theses and student projects for the robotics course. He has been serving as an Associate Editor for ICRA and ICORR Conferences, since 2015, and an Editor for *Actuators* (MDPI), *Robotics* (Cambridge), and Springer IJRR journals.

MANUEL G. CATALANO (Member, IEEE) received the Laurea degree in mechanical engineering and the Ph.D. degree in robotics and bioengineering from the E. Piaggio Research Center, University of Pisa.

He is currently a Researcher with IIT under the research line SoftRobotics for Human Cooperation and Rehabilitation. He is also a Research Fellow with the Centro di Ricerca E. Piaggio, University of Pisa, and Mayo Clinic, Rochester, NY, USA. He is the Principal Investigator of the EU Project ''Reconcycle'' and coordinates the activities of the ''JOiiNT LAB,'' Bergamo, a technology transfer collaboration between IIT and Intellimech, a Consortium of Medium and Big Mechatronic Enterprises.

ANTONIO BICCHI (Fellow, IEEE) graduated from the University of Bologna, in 1988.

He was a postdoc scholar at MIT Artificial Intelligence Laboratory. He teaches robotics and control systems with the Department of Information Engineering (DII), University of Pisa. He leads the Robotics Group, Research Center ''E. Piaggio,'' University of Pisa, since 1990. Since 2013, he has been an Adjunct Professor with the School of Biological and Health Systems Engineering, Arizona State University. He is currently a Professor of robotics with the University of Pisa and a Senior Scientist with Italian Institute of Technology, Genoa. He is the Head of the Soft Robotics Laboratory for Human Cooperation and Rehabilitation, IIT, Genoa. He is a co-founder and has been the President of the Italian Institute of Robotics and Intelligent Machines (I-RIM) since 2019. He is the Scientific Coordinator of JOiiNT LAB, an advanced tech transfer laboratory with leading-edge industries in Bergamo, Italy. He has published more than 500 papers in international journals, books, and refereed conferences. His research on human and robot hands has been generously supported by European Research Council with an Advanced Grant, in 2012, a Synergy Grant, in 2019, and three Proof-of-Concept grants. His main research interests include robotics, haptics, and control systems.

Mr. Bicchi organized the first World Haptics Conference, in 2005, today the premier conference in the field. From January 2023, he was the Editor-in-Chief of *The International Journal of Robotics Research* (IJRR) and the first scientific journal in *Robotics*. He has been the Founding Editor-in-Chief of the IEEE Robotics and Automation Letters, from 2015 to 2019, which rapidly became the top *Robotics* journal by number of submissions.

Open Access funding provided by 'Università di Pisa' within the CRUI CARE Agreement